X-Ray Study of the Nematic Phase and Smectic-A_1–to–Smectic-$\tilde{A}$ Phase Transition in Heptylphenyl Nitrobenzoloxybenzoate ($DB7NO_2$)

C. R. Safinya, William A. Varady, L. Y. Chiang, and P. Dimon

Corporate Research Science Laboratories, Exxon Research and Engineering Company, Annandale, New Jersey 08801

(Received 8 November 1986)

We report a high-resolution x-ray study of the fluctuations in the nematic and smectic-A_1 phases in heptylphenyl nitrobenzoloxybenzoate. As a function of decreasing temperature, the fluctuations evolve from an incommensurate region, through an intermediate region of coexisting (competing) incommensurate and smectic-$\tilde{C}$ fluctuations, to a region dominated by pretransitional smectic-$\tilde{A}$ fluctuations which exhibit a phase-lockin smectic-A_1–smectic-$\tilde{A}$ transition. This behavior directly confirms the current theoretical description of the smectic-$\tilde{A}$ and smectic-$\tilde{C}$ phases as alternatives to the incommensurate phase.

PACS numbers: 64.70.Md, 61.30.Eb

The smectic-A (SmA) phase of liquid crystals consists of oriented molecules segregated into stacks of two-dimensional liquid layers with spacing d. Recently, considerable experimental[1–3] and theoretical[4,5] effort has been concentrated on the understanding of the nature of the phases and transitions of an entirely new class of polar liquid crystals with competition between two different layer spacings in SmA phases. In the SmA_1 (monolayer) phase, the polar molecules are randomly up and down in each layer and the one-dimensional density wave has periodicity $d_2 = l$ = molecular length. The SmA_2 bilayer (antiferroelectric) phase consists of layers in which the molecules are preferentially up or down and the density wave has period $d_1 = 2l$ commensurate with the molecular length. Previous[1] low-resolution x-ray work has also revealed novel Sm$\tilde{A}$ and Sm$\tilde{C}$ antiphase structures in which the direction of the dipolar molecule is modulated in the plane of the layers (top, Figs. 2 and 4).

To describe these phases within a unified framework, Prost and Barois[4] (P-B) proposed a phenomenological model with Ψ_2 and Ψ_1, characterizing the density and the antiferroelectric order parameters. As essential ingredients, the model incorporates two types of important terms: first, the elastic terms, $|(\nabla^2 + k_1^2)\Psi_1|^2$ and $|(\nabla^2 + k_2^2)\Psi_2|^2$, which describe spatial modulations with preference to order at incommensurate wave-vector moduli $|\mathbf{k}_1| = 2\pi/l'$ $(l' < 2l)$ and $|\mathbf{k}_2| = 2\pi/l$; and second, the coupling term $\Psi_1^2\Psi_2^*$ which favors the lockin (commensurability) of $\mathbf{k}_1$ and $\mathbf{k}_2$. These opposing tendencies lead to frustration and the system responds with the formation of various SmA phases. In the model, for one-dimensional modulations, either a commensurate phase is stabilized when the lockin term dominates, or an incommensurate (I) phase when the elastic terms dominate. To date, however, while the SmA_2 commensurate phase has been observed in numerous systems,[1] there is only one very recent report[3] of the possible existence of an ordered (I) phase in a binary mixture in which two density waves with incommensurate period coexist. To explain this scarcity, Prost and Barois hypothesize that in most systems, the smectic antiphases ($\tilde{A}$ and $\tilde{C}$) will be preferred to the incommensurate phase because the phases compromise between the elastic and commensurability energies. For example, in the Sm$\tilde{A}$ phase, the antiferroelectric incommensurate modulation at $\mathbf{k}_1$ tilts away from the z axis [developing an in-the-layer component $\mathbf{k}_1 = k_{1z}\hat{\mathbf{z}} + k_{1\perp}\hat{\mathbf{e}}_\perp$—see Fig. 2 (top)] with k_{1z} locked ($2k_{1z} = 2q_0$) onto the monolayer modulation at $\mathbf{k}_2 = 2q_0\hat{\mathbf{z}}$. This configuration simultaneously minimizes the commensurability energy and preserves modulus $|\mathbf{k}_1|$ favored by the elastic terms. Wang and Lubensky[5] (W-L) studied the density fluctuations in the monolayer SmA_1 phase using the P-B model as a starting point. Significantly, they predict that the competition between the incommensurate (I) phase and the Sm$\tilde{A}$ antiphase may be directly observable as a region of coexisting I and Sm$\tilde{A}$ fluctuations.

To elucidate the problem and understand the nature of the onset of antiphase ordering, we carried out a a high-resolution x-ray study of the density fluctuations in the nematic (N) and SmA_1 phases ($T_{NA_1} = 96.90\,^\circ\mathrm{C}$) associated with the Sm$A_1$–Sm$\tilde{A}$ transition ($T_{A_1\tilde{A}} = 92.21\,^\circ\mathrm{C}$) in the compound nitrobenzoloxybenzoate of heptylphenyl[1] ($DB7NO_2$). Our most important result is that the crossover from incommensurate (I) to Sm$\tilde{A}$ antiphase fluctuations in $DB7NO_2$ does in fact occur through a region of coexisting incommensurate and antiphase fluctuations directly confirming the competition between these fluctuations. This then strongly supports the Prost-Barois hypothesis that the smectic antiphases are alternatives to the I phase.

The experiments were carried out on a rotating-anode x-ray source with use of Ge(111) crystals as

monochromator and analyzer elements. The resolution expressed in terms of the half width at half maximum (HWHM) was 4.2×10^{-4} Å^{-1} in the longitudinal direction, and $<2\times10^{-5}$ Å^{-1} in the transverse in-plane and 5×10^{-3} Å^{-1} in the transverse out-of-plane directions. An applied magnetic field of 3.0 kG provided alignment of the nematic director in the scattering plane. A two-stage oven provided temperature control of ±2.5 mK.

We begin with the behavior in the nematic phase. The critical scattering associated with the onset of a one-dimensional density wave with monolayer periodicity at the nematic-SmA_1 transition is centered about $\mathbf{k}_2=(0,0,2q_0=2\pi/l=0.2298$ Å$^{-1})$ in reciprocal space. Simultaneously, a second incommensurate density fluctuation with period less than the antiparallel pair length is centered about $\mathbf{k}_1=(0,0,k_1=(1+\epsilon_1)q_0)$ with the incommensurability parameter ϵ_1 decreasing from 0.23 to 0.16 in the N phase. The scattering is shown schematically at the top of Fig. 1 with the nematic director along $\hat{\mathbf{z}}$. For each temperature, we carried out a complete series of longitudinal ($q_\parallel$ varied, $\parallel=z$) and transverse ($q_\perp$ varied) scans mapping out the entire scattering plane in the vicinity of $\mathbf{k}_1$ and $\mathbf{k}_2$. We show in Fig. 1(a) longitudinal scans in the nematic phase through $(0,0,k_1)$ and $(0,0,k_2)$ at three temperatures $T-T_{NA_1}=10.90\,^\circ$C, $1.10\,^\circ$C, and $0.085\,^\circ$C ($T_{NA_1}=96.90\,^\circ$C) as the SmA_1 phase is approached. Quantitatively the scattering may be described by an x-ray structure factor[6] centered at $(0,0,k_1)$ and $(0,0,k_2)$:

$$S(\mathbf{q})=\sum_{i=1}^{2}\frac{S_{0,i}}{1+\xi_{\parallel,i}^2(q_\parallel-k_i)^2+\xi_{\perp,i}^2q_\perp^2+d\xi_\perp^4q_\perp^4}. \tag{1}$$

The solid lines through the data of Fig. 1(a) are the results of a fit of Eq. (1), convoluted with the instrumental resolution, to longitudinal and transverse scans through $\mathbf{k}_1$ and $\mathbf{k}_2$. This yields susceptibilities $S_{0,i}$ and correlation lengths $\xi_{\parallel,i},\xi_{\perp,i}$ for the incommensurate ($i=1$) and monolayer ($i=2$) density fluctuations. At the N-SmA_1 transition, the monolayer density wave at $\mathbf{k}_2$ condenses with diverging susceptibility $S_{0,2}$ [Fig. 1(b)] and correlation lengths similar to previous N-SmA[6] transitions studied. Very importantly, the incommensurate density wave at $\mathbf{k}_1$ exhibits significant temperature dependence in the nematic phase [Fig. 1(a)] with the susceptiblibity $S_{0,1}$ and correlation lengths $\xi_{\parallel,1},\xi_{\perp,1}$ exhibiting broad maxima about one degree above the NA_1 transition as plotted in Figs. 1(b) and 1(c). Thus, as the temperature is decreased in the N phase, this behavior at $\mathbf{k}_1$, which indicates the approach towards an ordered incommensurate phase, is preempted (presumably because of the cost in lockin energy) just above the SmA_1 phase by a crossover to a

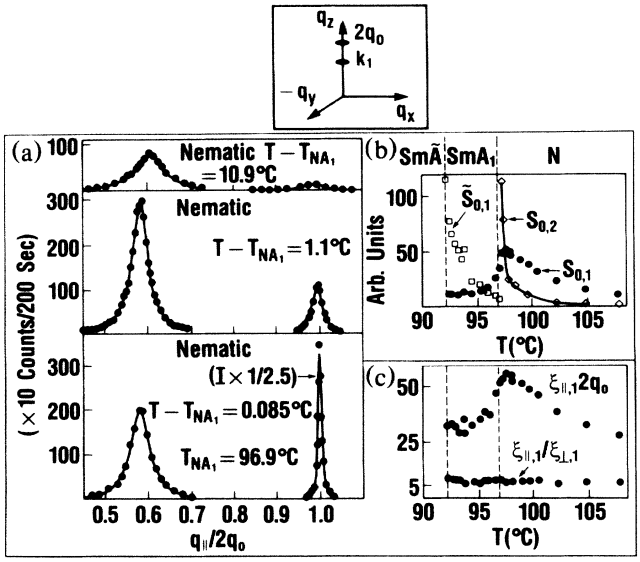

FIG. 1. Top: Nematic-phase scattering spectrum in reciprocal space with diffuse spots at incommensurate $\mathbf{k}_1$ and $\mathbf{k}_2=2q_0\hat{z}$. (a) Longitudinal scans through $\mathbf{k}_1$ and $\mathbf{k}_2$. The solid lines are the results of fits of Eq. (1) to the data. (b) Susceptibilities for the monolayer $S_{0,2}$, incommensurate $S_{0,1}$, and antiphase $\tilde{S}_{0,1}$ fluctuations. (c) Correlation length $\xi_{\parallel,1}$ and the ratio $\xi_{\parallel,1}/\xi_{\perp,1}$ for the incommensurate fluctuation.

region of coexisting incommensurate and antiphase fluctuations. Before describing this region, we first briefly discuss the limiting Sm$\tilde{A}$ fluctuation behavior near the SmA_1-Sm$\tilde{A}$ transition.

In the SmA_1 phase, the scattering exhibits a Bragg spot at $\mathbf{k}_2=(0,0,2q_0)$ and diffuse scattering near q_0. In the vicinity of the SmA_1-Sm$\tilde{A}$ transition, the diffuse scattering is dominated by Sm$\tilde{A}$ fluctuations. We show schematically at the top of Fig. 2 the real-space centered rectangular Sm$\tilde{A}$ unit cell.[1] The Sm$\tilde{A}$ fluctuation in the SmA_1 phase manifests itself as a ring of scattering at $\mathbf{k}_{\tilde{A}}=(k_\perp\cos\psi,k_\perp\sin\Psi,k_\parallel)$, $0\le\Psi\le2\pi$, in reciprocal space. Shown in Fig. 2 are the results of four (series of $q_\parallel$ and $q_\perp$) mesh scans near the bilayer wave vector q_0 plotted as equal intensity contours in the nematic phase [Fig. 2(a)] and in the SmA_1 phase [Figs. 2(b)–2(d)]. For symmetry reasons we show only $q_\parallel>0$ and $q_\perp>0$. We see that the single-spot pattern characteristic of incommensurate fluctuations at $\mathbf{k}_1=(0,0,k_1=(1+\epsilon_1)q_0;\ \epsilon_1\sim0.2)$ in the nematic phase [Fig. 2(a)] crosses over to a single-ring pattern indicative of pretransitional Sm$\tilde{A}$ fluctuations near the SmA_1-Sm$\tilde{A}$ transition [Fig. 2(d)] at $k_{\tilde{A}}=(k_\perp,0,k_\parallel=q_0(1+\epsilon))$ with very small incommensurability $\epsilon\simeq0.01$.

The evolution of the fluctuations from incommensurate to Sm$\tilde{A}$ behavior occurs through an intermediate region as we now discuss. As the incommensurate

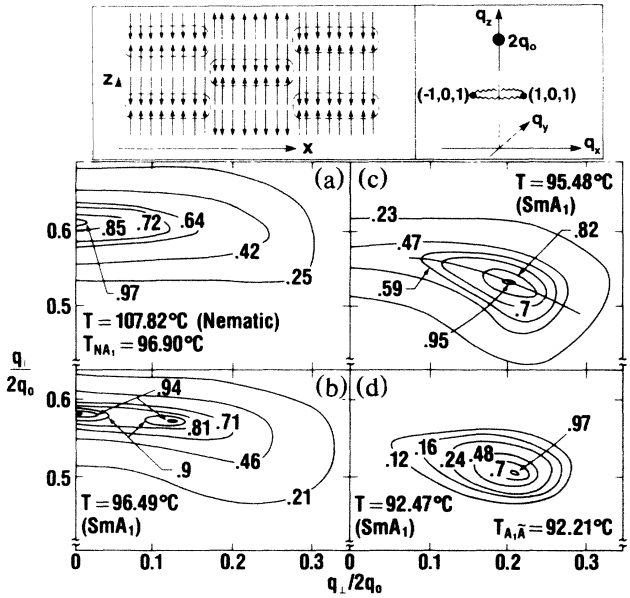

FIG. 2. (Top, left) Centered rectangular unit cell associated with short-range antiferroelectric Sm$\tilde{A}$ order (arrows indicate polar end) and (right) resulting diffuse ring in reciprocal space in the Sm$\tilde{A}$ phase. [Bottom, (a)–(d)]: Contour plots showing the evolution of scattering near the bilayer q_0 position in the nematic and smectic-A_1 phases as discussed in the text.

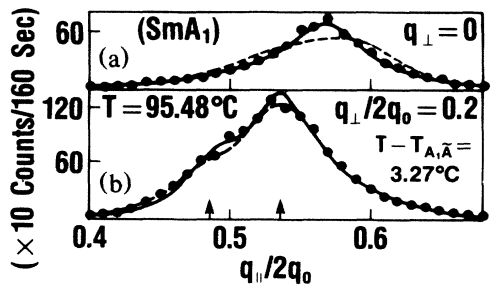

FIG. 3. Longitudinal scans through the center ($q_\perp = 0$) and peak ($q_\perp/2q_0 = 0.2$) of the ring pattern of Fig. 2(c). The dashed lines are fits by Eq. (2) and the solid lines are fits by a sum of Eq. (2) and Eq. (1) (for $i = 1$) (see text).

susceptibility $S_{0,1}$ decreases [Fig. 1(b)], antiphase fluctuations set in near the N-SmA_1 transition. We show in Fig. 2(b) the contour plot of *coexisting incommensurate and antiphase fluctuations* at $T = 96.49\,^\circ\text{C} = T_{NA_1} - 0.41\,^\circ\text{C}$ where the scattering into the spot and antiphase ring are comparable. At this temperature, the precise nature of the antiphase fluctuation is masked by the presence of strong incommensurate scattering. As the temperature is further decreased, we see that at $T = 95.48\,^\circ\text{C} = T_{NA_1} - 1.42\,^\circ\text{C}$, the contour plot of Fig. 2(c) shows the ring pattern clearly. Qualitatively, two features become apparent. First, the fluctuations in the SmA_1 phase appear to occur on a constant $|\mathbf{q}|$ radius in reciprocal space [solid radial line, Fig. 2(c)]. Second, the contour lines appear asymmetrically about this radial line; that is, the distances from the peak position to equal intensity contours above and below this line along $q_\parallel$ are not equal. A single-ring pattern which is the behavior near the SmA_1-Sm$\tilde{A}$ transition shown in Fig. 2(a) does not exhibit this asymmetry. This second feature is elucidated in Fig. 3, where we show longitudinal ($q_\parallel$) scans through the peak $q_\perp/2q_0 = 0.2$ and center $q_\perp = 0$ of the ring pattern of Fig. 2(c). The scan through the ring maximum [Fig. 3(b)] reveals a double-peak structure (arrows mark the peak positions). In this temperature range, the antiphase fluctuation is manifested as two closely spaced rings, which is characteristic of Sm$\tilde{C}$ fluctuations.[4,5]

We show schematically at the top of Fig. 4 the real-space unit cell of the oblique centered Sm$\tilde{C}$ lattice which can be thought of simply as a "sheared Sm$\tilde{A}$." This structure gives rise to (1,0,1) and (−1,0,1) reflections with unequal wave-vector moduli which, when azimuthally averaged, give rise to two rings in

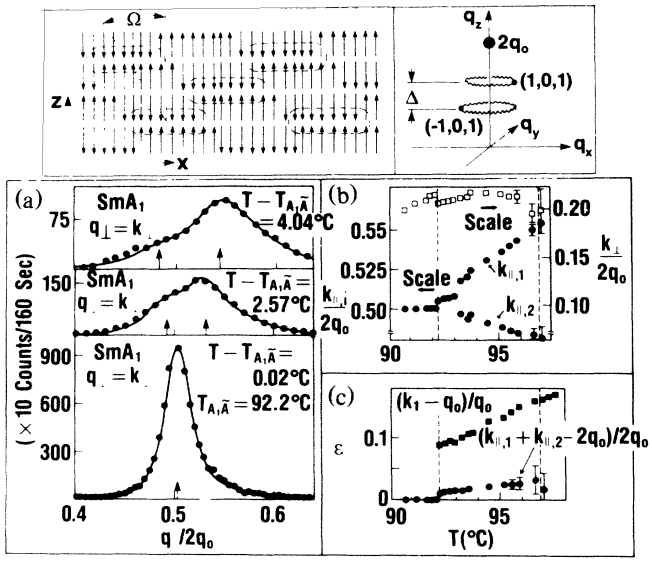

FIG. 4. (Top, left) Centered oblique unit cell (arrows indicate polar end) associated with short-range Sm$\tilde{C}$ order and (right) resulting diffuse double ring in reciprocal space in the SmA_1 phase. (a) Longitudinal scans through the peak of the double-ring Sm$\tilde{C}$ (top and center) and single-ring Sm$\tilde{A}$ (bottom) diffuse scattering profile. Solid lines are result of fits (see text). (b) Longitudinal ($k_{\parallel,1}$ and $k_{\parallel,2}$) and transverse ($k_\perp$) peak positions of the double-ring (Sm$\tilde{C}$) followed by single-ring (Sm$\tilde{A}$) scattering. (c) Incommensurability parameter for the incommensurate (solid square) and antiphase Sm$\tilde{C}$ and Sm$\tilde{A}$ (solid circle) fluctuations. The vertical dashed lines give the N-SmA_1 and SmA_1-Sm$\tilde{A}$ phase boundaries.

reciprocal space (top, Fig. 4).

The double-peaked Sm$\tilde{C}$ scattering may be quantitatively described by the sum of two rings:

$$S(\mathbf{q}) = \sum_{i=1}^{2} \frac{\tilde{S}_{0,i}}{1+\xi_{\parallel}^2 q_{\parallel,i}'^2 + \xi_{\perp}^2 q_{\perp}'^2 + d_{\parallel} q_{\parallel,i}'^4 + d_{\perp} q_{\perp,i}'^4 + c q_{\parallel,i}' q_{\perp}'} \tag{2}$$

with $q_{\parallel,i}' = q_{\parallel} - k_{\parallel,i}$, $q_{\perp}' = q_{\perp} - k_{\perp}$, and where $k_{\parallel,1}$ and $k_{\parallel,2} = k_{\parallel,1} - \Delta$ and $\tilde{S}_{0,1}, \tilde{S}_{0,2}$, are the longitudinal peak positions and the amplitudes, respectively, of the upper and lower rings [$\mathbf{k}(101)$ and $\mathbf{k}(-101)$ reflections shown schematically at the top of Fig. 4] separated by Δ. The data require non-negligible quartic terms. The lowest-order cross term is needed to characterize the approximately radial nature of the fluctuations [Figs. 2(c) and 2(d)]. This finding supports one of the important assumptions of the P-B and W-L models which introduce elastic terms of the type $|(\nabla^2 + k_1^2)\Psi_1|^2$ to indicate the preference of Ψ_1 to order at $|\mathbf{k}_1|$; these terms, in turn, lead to the prediction[5] of the radial nature of $S(\mathbf{q}) \sim \langle \Psi_1(\mathbf{q})\Psi_1(-\mathbf{q})\rangle$. Equation (2), which characterizes the double-ring scattering, cannot simultaneously describe the scattering away from the ring maxima near the incommensurate peak at $\mathbf{k}_1 = (0,0,k_1)$. This is quantitatively evident from Fig. 3, where the dashed line is a fit of Eq. (2) to simultaneous longitudinal scans around the ring maximum at $q_{\perp}/2q_0 = 0.2$, which describes the double ring accurately [Fig. 3(b)], but not the scattering through $q_{\perp} = 0$ [Fig. 3(a)], which is significantly narrower. The solid line is a best fit ($\chi^2 \sim 2$) of $q_{\parallel}$ and $q_{\perp}$ scans spanning the entire fluctuation range to a sum of Eq. (2) and Eq. (1) (for $i = 1$) characterizing an intermediate region of coexisting Sm$\tilde{C}$ and incommensurate (I) fluctuations. I fluctuations appear to persist even near the SmA_1-Sm$\tilde{A}$ transition.

As the temperature is decreased in the SmA_1 phase, we find that the Sm$\tilde{C}$ fluctuations evolve continuously into Sm$\tilde{A}$ fluctuations. We show in Fig. 4(a) longitudinal scans through the double-ring maximum at $q_{\perp} = k_{\perp}$ which indicate that the separation $\Delta = k_{\parallel,1} - k_{\parallel,2}$ between the longitudinal peak positions (marked by arrows) decreases with an eventual collapse ($\Delta = 0$) of the rings above the weakly first-order SmA_1-Sm$\tilde{A}$ transition. We plot the peak positions $k_{\perp}$, $k_{\parallel,1}$, and $k_{\parallel,2}$ of the antiphase scattering as a function of temperature in Fig. 4(b) which corresponds to Sm$\tilde{C}$ fluctuations with an oblique angle $\Omega = \tan^{-1}(\Delta/2k_{\perp})$ (Fig. 4, top) that continuously shear to the Sm$\tilde{A}$ ($\Delta, \Omega = 0$) configuration (Fig. 2, top) about 0.75 °C above the Sm$\tilde{A}$ phase. In the P-B model the coupling term $\sim \Psi_1^2 \Psi_2^*$ leads to a commensurability energy which is minimum for $\mathbf{k}_2 (= 2q_0\hat{z}) = \mathbf{k}(101) + \mathbf{k}(-101)$. The Sm$\tilde{A}$ represents the symmetric case when $|\mathbf{k}(101)| = |\mathbf{k}(-101)|$ (Fig. 2, top). For the Sm$\tilde{C}$, $|\mathbf{k}(101) \neq |\mathbf{k}(-101)|$ (Fig. 4, top). *Significantly, we find that the incommensurability parameter* $\epsilon = (k_{\parallel,1} + k_{\parallel,2} - 2q_0)/2q_0$ *plotted in Fig. 4(c) associated with antiphase Sm$\tilde{C}$ and Sm$\tilde{A}$ fluctuations is small (< 0.02) over the entire SmA_1 phase and locks in ($\epsilon = 0$) across the SmA_1-Sm$\tilde{A}$ transition.* We also show $\epsilon_1(\mathrm{I}) = (2k_1 - 2q_0)/2q_0 \gtrsim 0.10$ associated with incommensurate fluctuations at $\mathbf{k}_1$ which are large only in the nematic phase. Thus, antiphase fluctuations, which set in this intermediate region, occur with $\epsilon \ll \epsilon_1$ reflecting the importance of the coupling term in the P-B and W-L models.

In conclusion, we find that the approach of incommensurate (I) fluctuations with large incommensurability $\epsilon_1 > 0.16$ towards ordering in the nematic phase is preempted by a crossover, through an intermediate region of coexisting I and Sm$\tilde{C}$ antiphase fluctuations, to a region dominated by Sm$\tilde{A}$ antiphase fluctuations with very small incommensurability $\epsilon \sim 0.01$ and exhibiting a lockin SmA_1-Sm$\tilde{A}$ transition. This intermediate region directly confirms the competition between I and Sm$\tilde{C}$ antiphase fluctuations and strongly supports the P-B hypothesis that the smectic antiphases are alternative to the I phase. Although the present W-L model predicts a coexisting region of I and Sm$\tilde{A}$ fluctuation rather than I and Sm$\tilde{C}$ which is what is observed in DB7NO$_2$, a more complete analysis which goes byeond the harmonic approximation should yield either type of antiphase fluctuations in the coexistence region.

We wish to thank S. Alexander, R. J. Birgeneau, N. A. Clark, C. C. Huang, and R. Pindak for stimulating discussions. One of us (C.R.S.) is particularly grateful to T. C. Lubensky and J. Prost for extensive conversations.

[1]F. Hardouin, A. M. Levelut, M. F. Archard, and G. Sigaud, J. Chim. Phys. **80**, 53 (1983); C. C. Huang, S. C. Lien, S. Dumrongrattana, and L. Y. Chiang, Phys. Rev. A **30**, 965 (1984).

[2]K. K. Chan, P. S. Pershan, L. B. Sorensen, and F. Hardouin, Phys. Rev. Lett. **54**, 1694 (1985).

[3]B. R. Ratna, R. Shashidhar, and V. N. Raja, Phys. Rev. Lett. **55**, 1476 (1985).

[4]J. Prost and P. Barois, J. Chim. Phys. **80**, 65 (1983); J. Prost, Adv. Phys. **33**, 1–46 (1984).

[5]J. Wang and T. C. Lubensky, J. Phys. **45**, 1653 (1984).

[6]R. J. Birgeneau, C. W. Garland, G. B. Kasting, and B. M. Ocko, Phys. Rev. A **24**, 2624 (1981).